# Optimization of quadrature frequency conversion with type-II KDP for second harmonic generation of the nanosecond chirp pulse at 1053 nm

**Lailin Ji (季来林)[1,2*], Baoqiang Zhu (朱宝强)[1], Chong Liu (刘 崇)[1], Tao Wang (王 韬)[2], and Zunqi Lin (林尊琪)[1],**

[1]*Shanghai Institute of Optics and Fine Mechanics, Chinese Academy of Sciences, Shanghai 201800, China*

[2]*Shanghai institute of laser plasma, Chinese academy of engineer and physics, Shanghai 201800, China*

[*]*Corresponding author: jsycjll@siom.ac.cn*

Received October 7, 2013; accepted January 22, 2014; posted online February 28, 2014

A second harmonic generation system with two type II KDP crystals in quadrature is optimized for the nanosecond chirp pulse. The acceptance bandwidth of this optimizing scheme is close to 10 nm by using two crystals with slightly opposite angular detuning from phase matching and the conversion efficiency can reach 70% for top-hat chirp pulse at ∼2 GW/cm$^2$ in theory. The preliminary experimental results are obtained on the 9th beam of Shen Guang II SGII laser system, and the performance of optimization is partially verified.

*OCIS codes:* 190.2620, 190.4360.
*doi: 10.3788/COL201412.031902.*

The Nd: glass laser system has been used for inertial confinement fusion (ICF) studies over 30 years. The typical system is the National Ignition Facility (NIF), the third harmonic (351 nm) energy can reach 1.8 MJ, over 500 TW. However some difficulties arise from laser plasma instability (LPI) in the experiments, the energy loss is higher than expected and damage to the fused silica optics in $3\omega$ is very severe. As described in a recent publication, the possibility of using the second harmonic (SH) has been a research hotspot for some time[1−3]. This plan has two merits. First, the damage threshold of fused silica optics increases with increasing wavelength, and the SH energy can be increased to approximately twice the third ones. Second, the SH bandwidth can reach terahertz magnitude, which is very useful for the suppression stimulated Brillouin scattering, stimulated Raman scattering, and filament in plasma (requires a ∼1000-GHz spectrum)[4]. Bandwidths of up to 1 THz are readily achievable in Nd: glass laser systems in the spectral region near 1 $\mu$m with the optical parametric chirped pulse amplification (OPCPA). For instance, the bandwidth of the nanosecond chirp pulse of 1053 nm on Shen Guang II (SGII) No. 9 is about 950 GHz ($\Delta\lambda_{\mathrm{FWHM}}$ ∼3.5 nm), the Gaussian pulse duration $\tau_{\mathrm{FWHM}}$ is around 1.5 ns, and the output energy can up to ∼2000 J with Φ310-mm aperture. Recently, physicists have suggested using the SH of this chirp pulse to investigate LPI. Accordingly, the SH generation (SHG) system with two type-II KDP crystals in quadrature (Fig.1) is optimized. This scheme was firstly presented by Eimerl[5], and demonstrated by Pronko *et al.*[6] In contrast with other complexity and costly approaches, such as achromatic phase-matching (APM)[7,8], titled quasi-phase matched gratings[9], partially deuterated KDP[10], which have been tried to broaden the effective spectral acceptance bandwidth of SHG, the quadrature scheme is compatible with the high power Nd: glass laser system, and has been used for SHG with the beam of many longitudinal modes in Ref. [6].

In conventional single type-II KDP doubler, birefringence limits the intensity conversion to ∼50% at bandwidths of 2−3 nm for the large group velocity mismatch (GVM) between the two orthogonal components of the fundamental harmonic (FH) in ∼1-cm KDP[6,11]. The quadrature configuration compensates for this mismatch, because the transverse projections of the two crystal's principal axes are orthogonal, as shown in Fig. 1. So the fundamental component polarized along the slow axis in the first crystal was polarized along the fast axis in the second crystal as detailed in Ref. [6], when the thickness of the second crystal was twice of the first crystal, this compensation of GVM was obvious, it was helpful for SHG of a beam with a short coherence time ($\tau$ ∼1 ps), and energy conversion efficiencies ∼55% was obtained with an initial bandwidth for the fundamental of ∼2-nm full-width of half-maximum (FWHM). In this paper, the performance of this scheme was farther optimized with the detuned angle of the two crystal, and the acceptance bandwidth can be increased using two crystals with slightly opposite angular detuning from phase matching and suitable thicknesses, which is a customary method for the large bandwidth pulse, such as in Refs. [12,13]. A simple physical explanation exists for the increased bandwidth converted with this optimization. The first crystal more efficiently converts positive frequencies (fall edge of the chirp pulse in this article) than negative frequencies (rise edge of the chirp pulse), as measured from the central frequency at which perfect type-II phase matching exists. Conversely, the second crystal, that is angle detuned in the opposite orientation, does the opposite. The two crystals in quadrature then convert a broad range of both positive and negative frequencies. Harmonic back-conversion for phase mismatching is

 

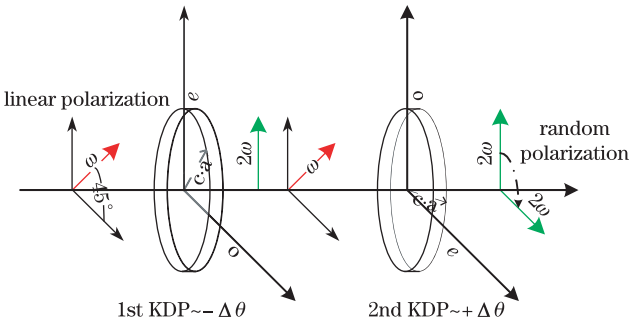


Fig. 1. Scheme of second harmonic generation with Type II KDP crystals in quadrature.

minimized because the SH generated in the first crystal is not at the correct polarization for interaction in the second crystal, different from the multi-crystal design in Refs. [11,12], where the distance between crystals should be carefully controlled to avoid the harmonic back-conversion.

This improvement is very helpful for the long chirp pulse, because the effect of temporal walking-off between the "o" and "e" beam is small for nanosecond chirp pulses, and the main reasons for the decreased conversion efficiency are non-uniformity profiles and phase mismatching caused by the broad bandwidth, beam divergence and so on. Its performance has been verified with the numerical simulation and experiments.

With the following definitions for the three fields[14]:

$$E_i = \frac{A_i(z,t)}{2\sqrt{n_j}} \exp[-\mathrm{i}(\omega_j t - k_j z)] + \mathrm{c.c}, \quad j = 1,2,3, \quad (1)$$

where $A_1$, $A_2$, and $A_3$ are the complex amplitudes of the fundamental "o" and "e" waves and the "e" polarized second harmonic wave, respectively. The relationship between intensity and electric field amplitude is $I_j(z,t)=(n_j\epsilon_0 c/2)\,|E_j(z,t)|^2 =(\epsilon_0 c/2)\,|A_j(z,t)|^2$, where $n_j$ is the refractive index of the involved waves in the phase-matching direction, and $\epsilon_0$ are the free space values of permittivity, and $c$ is velocity of the light in vacuum.

The three-wave nonlinear-coupled, which neglected the transverse effects, was used to simulate SHG with the quadrature scheme and has the form[6,11,15,16]:

$$\frac{\partial A_1}{\partial z}+\frac{1}{v_{g1}}\frac{\partial A_1}{\partial t}+\frac{\alpha_1}{2}A_1+\frac{\mathrm{i}}{2}g_1\frac{\partial^2 A_2}{\partial t^2}=\mathrm{i}KA_2^*A_3E^{\mathrm{i}\triangle kz}, \quad (2a)$$

$$\frac{\partial A_2}{\partial z}+\frac{1}{v_{g2}}\frac{\partial A_2}{\partial t}+\frac{\alpha_2}{2}A_1+\frac{\mathrm{i}}{2}g_2\frac{\partial^2 A_2}{\partial t^2}=\mathrm{i}KA_2^*A_3E^{\mathrm{i}\triangle kz}, \quad (2b)$$

$$\frac{\partial A_3}{\partial z}+\frac{1}{v_{g3}}\frac{\partial A_3}{\partial t}+\frac{\alpha_3}{2}A_3+\frac{\mathrm{i}}{2}g_3\frac{\partial^2 A_3}{\partial t^2}=2\mathrm{i}KA_2^*A_3E^{\mathrm{i}\triangle kz}, \quad (2c)$$

where $v_{gn} = \partial\omega_j/\partial k_n$ is the group velocity of the $n$th wave, $\alpha_j$ is the linear the absorption coefficients, $g_j = \partial^2 k_n/\partial\omega_j^2$ accounts for the group velocity dispersion, $\Delta k = k_1+k_2-k_3$ is the wave vector mismatch, $k$ is the field coupling coefficient and is expressed as

$$k = \frac{\omega}{c}\frac{d_{36}}{\epsilon_0}\frac{1}{\sqrt{n_1 n_2 n_2}}\sin(2\theta_m). \quad (3)$$

For a type-II SHG in KDP at the Nd:glass wavelength of $\lambda$=1053 nm , $\theta_m$ =58.9°, and $d_{36}/\epsilon_0$=0.39 pv/m[7,8].

The key parameters of Eq. (2) are illustrated in Table 1.

Temporal profiles were assumed to be supper-Gaussian (exponent = 40) at the entry of the first crystal, and the fields are expressed as follow

$$A_1 = A_2 = \frac{\sqrt{2}}{2}(2I_\omega/\,\epsilon_0\,c)^{\frac{1}{2}} \exp\Big(-0.5(\frac{t}{\tau/2})\Big)^{20}\exp(\mathrm{i}pt^2), \quad (4a)$$

$$A_3 = 0, \quad (4b)$$

where $\tau$= 1.5 ns is the pulse duration and $p$=6000 rad/ns$^2$ is the parameter of chirp pulse; $I_\omega$ is the full intensity of the input field of 1053 nm, and the electromagnetic polarized at an angle of 45° to the o-direction is incident on the first crystal, and the ratio of "$A_1$" to "$A_2$" is 1:1. The loss of the surface reflectivity is about 2 percent/surface at FH and SH, it also has been taken into account in calculation process. The phase $\phi(t)$ of input pulse has a quadratic form in Eq. (4a), and the spectrum profile has a top-hat form, and the bandwidth is 2700 GHz (10 nm) in theoretical calculations. It is convenience to observe the altering of spectrum in the SHG process with this hypothesis. Notably the output fields of the "o" and "e" from the first crystal will be the "e" and "o" in the second crystal.

**Table 1. Key Parameters of Eq. (2)**

| | $N$ | $v_{gj}$ ($\times10^8$m/s) | $g_j$ ($\times10^{-6}$ps$^2$/cm) | $\alpha_j$ (cm$^{-1}$) |
|---|---|---|---|---|
| $\omega$(o) | 1.494 | 1.967 | −2.4 | 0.058 |
| $\omega$(e) | 1.469 | 2.02 | 2.2 | 0.02 |
| 2$\omega$(e) | 1.482 | 1.989 | 13.6 | – |

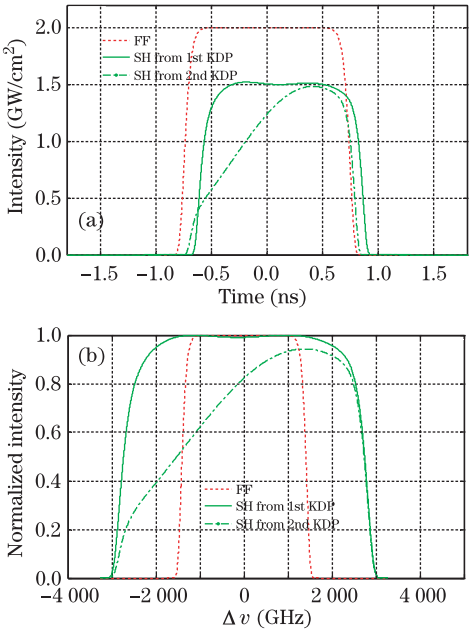


Fig. 2. (a) Intensity temporal and (b) spectral profiles of FH (red dotted curve) incident upon the first KDP, together with the SH emerging from the first (green dashed curve) and the second KDPs (green solid curve).

According to the simulation, the optimized scheme chose for the chirp pulse is as follows. The thickness of the first crystal is 10 mm, and the thickness of the second crystal is 14 mm. The first crystal is detuned by 350 $\mu$rad (to phase match at 1050.5 nm), and the second was detuned by $-350\mu$ rad (to phase match at 1055.5 nm).

Figure 2 shows the temporal and spectrum profiles of SH emerging from the first and the second KDP crystals. The back of the chirp pulse is found to be efficiently converted to the SH in the first KDP, and the leaving part is efficiently converted to the SH in the second KDP. The conversion efficiency is ~55% in the first crystal, and the total conversion efficiency of two crystals is about ~72%. And the SH emerging from the second KDP is the random polarization, it is helpful to reduce the beam coherence for beam smoothing[16].

The performance of this optimized quadrature scheme is compared with the conventional 14-mm type II KDP with compensation of the GVM by the first KDP. In the calculation, the first KDP is detuned 30 mrad, and the conversion efficiency can be neglected, but it can partially compensate the GVM in the second KDP as discussed in Refs. [5]. The second KDP is detuned 0°, and the SH temporal profiles and spectrum of 14-mm type II KDP are shown in Fig. 3. The temporal profile of SH with the 14-mm KDP is in a considerably distorted form, and the bandwidth of the SH is ~4000 GHz (4 nm). By contrast, scarcely distortion of the quadrature scheme is observed, and the output bandwidth is ~5400 GHz (5 nm) in Fig. 3.

Figure 4 shows the conversion efficiencies for different incident intensities of these two schemes. According to the simulation, it is found that the highest conversion

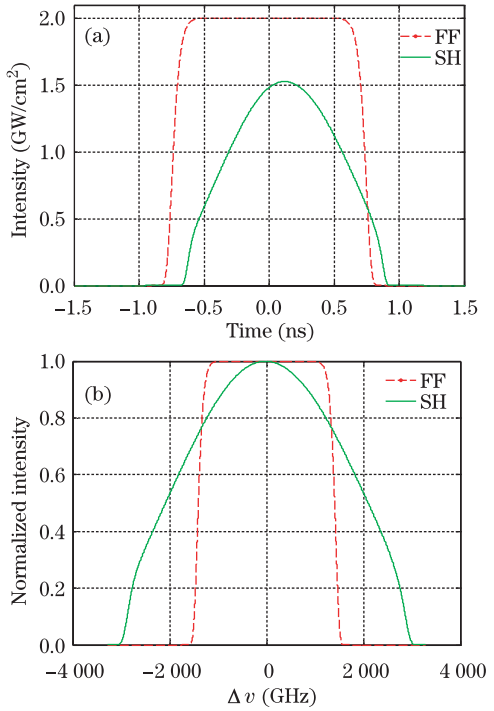


Fig. 3. (Color online) (a) Temporal and (b) spectral profile of the SH (green solid curve) emerging from 14-mm type II KDP, together with the FH (red dashed curve). The first KDP is detuned 30 mrad, and the second KDP keeps phase matched.

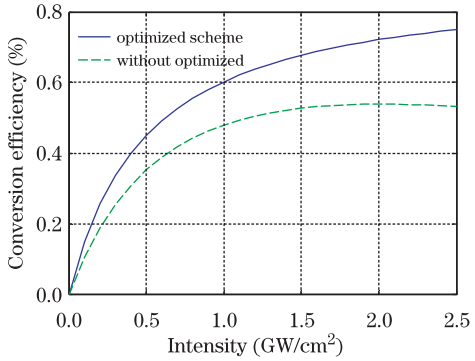


Fig. 4. Conversion efficiencies of the optimized scheme (blue solid curve) and 14-mm type II KDP (green dashed curve) versus incident intensity of FH.

efficiency of 14-mm KDP is only ~55%. The conversion efficiency of the optimized scheme is obviously higher than the 14-mm crystal and increases by ~15% when the average intensity approaches ~2 GW/cm$^2$.

The main factor affecting the increase in conversion efficiency of this nanosecond pulse with the broad bandwidth is the larger acceptance bandwidth of the quadrature scheme. This phenomenon can be observed from the temporal shape and spectrum of the SH in Figs. 2 and 3. The spectrum of SH is nearly twice of the FH in the optimized scheme, and the time profile shows no distinct changes of this chirp pulse. This finding implies that the acceptance bandwidth of this optimized scheme is close to 10 nm at the Nd:glass wavelength of $\lambda$=1053 nm. With the numerical simulation, it is also found that the small angular misalignments, ~ ±30 $\mu$rad, can be tolerated for this optimized scheme, and the incident intensity has a small effect on the spectrum profile of SH. These advantages are very helpful to increasing conversion efficiencies and the stability in the operation.

The performance of the quadrature scheme was also experimentally verified on the 9th beam of the SGII laser system. With the optical parameter chirp-pulse amplification front-end and Nd:glass amplifiers, the large energy and broad bandwidth laser on the 9th beam of the SGII laser system was easily obtained. The output energy of the broad pulse from the optical parametric chirped pulse amplification (OPCPA) front-end is about ~ 1–2 mJ, and the bandwidth is about 1800 GHz (6.8 nm). The gain of the Nd:glass amplifiers is close to $10^6$ times, and the output energy of the chirp pulse approaches 2000 J with an aperture of Φ310 mm. Given the gain-narrowing effect in amplifiers, the output-pulse bandwidth is about 950 GHz (3.5 nm). The typically temporal pulse shapes and spectra of the chirp pulse emerging from the OPCPA front-end and Nd:glass amplifiers are illustrated in Fig. 5.

The near field of the FH shows non-uniformity, the average intensity within Φ 310-mm apertures is about 65 percent of the peak intensity, and it is one of the reasons for the low conversion efficiencies in the experiment. The maximum average intensity across the beam is about 1.5 GW/cm$^2$. Measurements of the focal diameter indicated that 80% energy was within 8 times the diffraction limit. It was of adequate quality to perform the conversion efficiency measurements.

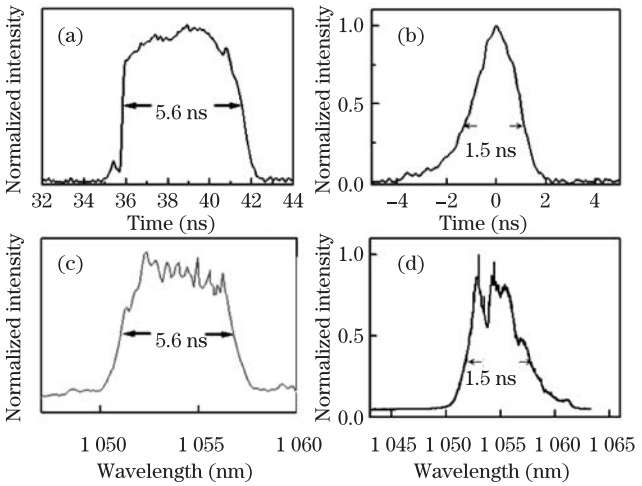


Fig. 5. Temporal shape and spectrum of the output pulse of OPCPA front-end and Nd:glass amplifiers. (a, c) OPCPA and (b, d) Nd:glass amplifiers.

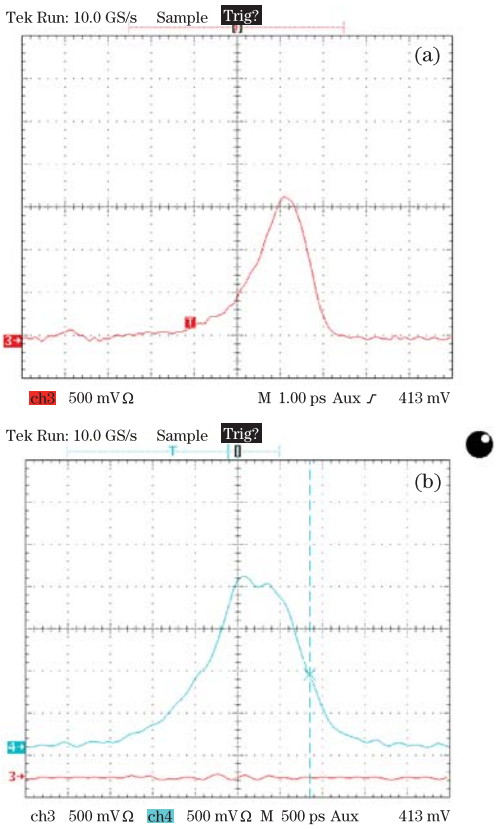


Fig. 6. (Color online) Typical temporal profiles of (a) input FH (red curve) and (b) output SH (blue curve) in the experiments.

The SHG system is composed of two type II KDP with an aperture of Φ380 mm. The first crystal is 11 mm with a detuned angle of approximately ∼ −350 μrad and the second crystal is 13 mm with a detuned angle of approximately ∼350 μrad. The detuned angle is controlled by step motor with an accuracy of ∼ 30 μrad, including the alignment error. This scheme is admittedly not the best, but is readily available in our laboratory. Its total conversion efficiency is nearly closed to the optimization scheme in Fig. 4, but the spectrum of SH is slightly asymmetric for the relatively higher conversion efficiency in the first crystal and the relatively lower conversion efficiency in the second crystal.

The typical temporal profiles of the FH and corresponding SH in the experiments are shown in Fig. 6. The pulse duration (FWHM) of FH is ∼1.35 ns, and the pulse duration of SH is ∼1.16 ns. Figure 9 shows the simulation of the temporal and spectral profile for this chirp Gaussian pulse, the pulse duration of the SH shortens to 1.2 ns, which is caused by the Gaussian envelop, because the conversion efficiency is falling with decreasing the intensity. It is also found that the central frequency of the output pulse has a slight fluctuation in the experiment, which may be caused by the instability of the central frequency in OPA frontend, but the central frequency shifting of the output pulse is not obvious, it is within 0.5 nm. The optimized quadrature scheme has a larger acceptance bandwidth of ∼10 nm, which can be seen in Fig. 2, so this fluctuation can be tolerant, and has no obvious effect on the performance of the conversion in the experiments.

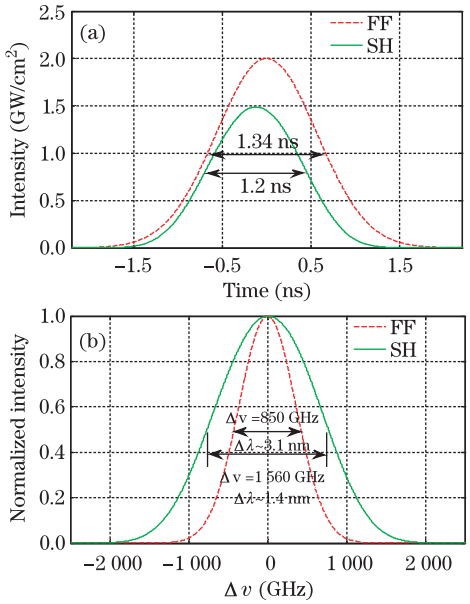


Fig. 7. (Color online) (a) Simulation temporal and (b) spectral profiles of the SH (green curve) with Gaussian chirp pulse (red dashed curve) emerging from the quadratic scheme.

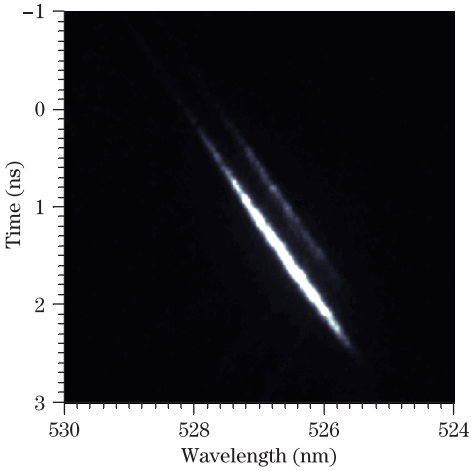


Fig. 8. Temporal and spectral characterizations of SH taken by spectral-resolved streak camera.

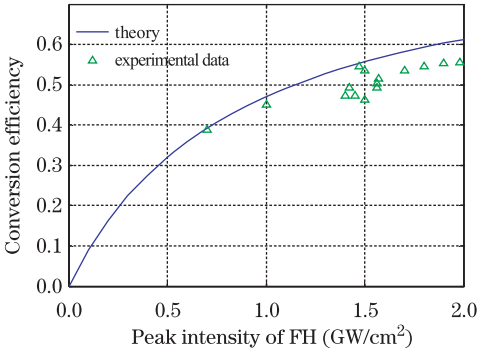


Fig. 9. Conversion efficiency measured for the quadrature scheme in the experiments.

The spectral characteristics of SH taken with spectral-resolve streak camera[18−20] has been illustrated in Fig. 8. It is found that the majority of the FH is converted to the SH in the first KDP, and the front of the pulse is efficiently converted to the SH in the second KDP as theoretical calculation. It indicates that the detuned angle play an effect on the conversion process as expectation, and the optimized scheme can be implemented in actually operation.

The data of the conversion efficiency as a function of the peak intensity at the FH is shown in Fig. 9, and it partially coincides with the theoretical result. The largest output energy of the SH is 827 J with a conversion efficiency of 55%. Despite the conversion efficiencies are limited by the Gaussian temporal envelope in the experiments, the preliminary experimental results indicate that the optimization of quadrature can be implemented on the facility to increase the acceptance bandwidth and conversion efficiencies of the process of SHG as the theoretical predication, and it can be used for SHG of the larger bandwidth chirp pulse with the theoretical calculation.

Although the performance of optimized quadrature scheme needs to be farther investigated, we believe that it is a well approach for SHG of broad bandwidth on high power laser facility with the numerical simulation and preliminary experimental results. The acceptance bandwidth of this optimal scheme is close to 10 nm by using two crystals with slightly opposite angular detuning from phase matching, and the conversion efficiency can reach 70 % for top-hat pulse at high intensity in theory. The preliminary experimental results is obtained on the SGII No.9 facility, the largest SH energy is up to ∼827 J with the conversion efficiency of 55 % for the Gaussian chirp pulse.

This work was supported by the National Science and Technology Major Project of the Ministry of Science and Technology of China under Grant No.1229241A00.

## References

1. G. M. Heestand, C. A. Haynam, P. J. Wegner, M. W. Bowers, S. N. Dixit, G. V. Erbert, M. A. Henesian, M. R. Hermann, K. S. Jancaitis, K. Knittel, T. Kohut, J. D. Lindl, K. R. Manes, C. D. Marshall, N. C. Mehta, J. Menapace, E. Moses, J. R. Murray, M. C. Nostrand, C. D. Orth, R. Patterson, R. A. Sacks, R. Saunders, M. J. Shaw, M. Spaeth, S. B. Sutton, W. H. Williams, C. C. Widmayer, R. K. White, P. K. Whitman, S. T. Yang and B. M. Van Wonterghem, Appl. Opt. **47,** 3494 (2008).
2. S. Atzeni, A. Marocchino, and A. Schiavi, Phy. Plasma. **19,** 090702 (2012).
3. L. J. Suter, S. Glenzer, S. Haan, B. Hammel, K. Manes, N. Meezan, J. Moody, M. Spaeth, and L. Divol, K. Oades and M. Stevenson, Phy. Plasma. **11,** 2738 (2004).
4. Z. Lin, A. Lei, W. Fan, S. Zhou, and L. Wang, High Power Laser Sci. Eng. **1,** 110 (2013).
5. D. Eimerl, IEEE J. Quantum Electron. **23,** 1361 (1987).
6. M. S. Pronko, R. H. Lehmerg, S. Obenschain, C. J. Pawley, C. K. Manka, and R. Eckrdt, IEEE J. Quantum Electron. **26,** 337 (1990).
7. O. E. Martínz, IEEE J. Quantum Electron. **25,** 2464 (1989).
8. B. A. Richman, S. E. Bisson, R. Trebino, E. Sidick and A. Jacobson, Opt. Lett. **23,** 497 (1998).
9. S. Ashihara, T. Shimura, and K. Kuroda, J. Opt. Soc. Am. B **20,** 853 (2003).
10. W. G. Zheng, L. J. Qian, P. Yuan, H. Luo, and H. Y. Zhu, Chin. Phy. Lett. **23,** 139 (2006).
11. U. K. Sapaev, J. Kutzner, and K. Finsterbusch, Optical and Quantum Electronics **37,** 515 (2005).
12. D. Eimerl, J. M. Auerbach, C. E. Barker, and D. Milam, Opt. Lett **22,** 1208 (1997).
13. A. Babushkin, R. S. Craxton, S. Oskoui, M. J. Guardalben, R. L. Keck, and W. Seka, Opt. Lett. **23,** 927 (1998).
14. R. S. Craxton, IEEE J. Quantum Electron. **17,** 1772 (1981).
15. D. Eimerl, J. M. Auerbach, W. Milonni, J. Mod. Opt. **42,** 1037 (1995).
16. P. W. Milonni, J. M. Auerbach, and D. Eimerl, Proc. SPIE **2633,** 230 (1997).
17. E. Lefebvre, R. L. Berger, A. B. Langdon, B. J. MacGowan, J. E. Rothenberg, and E. A. Williams, Physics of Plasma **5,** 2701 (1998).
18. X. D. Xie, X. Wang, Q. H. Zhu, X. M. Zeng, F. R. Wang, X. J. Huang, K. N. Zhou, F. Wang, D. B. Jiang, Z. Huang, L. Sun, H. Liu, X. D. Wang, W. Deng, Y. Guo, and X. M. Zhang, Acta. Phy. Sin. **56,** 6463 (2007).
19. Y. Wang, J. Yao, D. Xu, P. Zhao, and P. Wang, Chin. Opt. Lett. **4,** 419 (2006).
20. S. Zhang, L. Guo, M. Li, L. Zhang, X. Yan, W. Hou, X. Lin, and J. Li, Chin. Opt. Lett. **10,** 071401 (2012).